Physics of the Earth and Planetary Interiors, 61 (1990) 269–290
Elsevier Science Publishers B.V., Amsterdam – Printed in The Netherlands

Earthquake source processes and subduction regime in the Santa Cruz Islands region

Fumiko Tajima [1], Larry J. Ruff [2], Hiroo Kanamori [3], Jiajun Zhang [3] and Kiyoo Mogi [4]

[1] *Institute for Geophysics, University of Texas, Austin, TX 78759 (U.S.A.)*
[2] *Department of Geological Sciences, University of Michigan, Ann Arbor, MI 48109 (U.S.A.)*
[3] *Seismological Laboratory, California Institute of Technology, Pasadena, CA 91125 (U.S.A.)*
[4] *Earthquake Research Institute, Tokyo University, Bunkyo-ku, Tokyo 113 (Japan)*

(Received September 28, 1989; accepted November 8, 1989)

Tajima, F., Ruff, L.J., Kanamori, H., Zhang, J. and Mogi, K., 1990. Earthquake source processes and subduction regime in the Santa Cruz Islands region. Phys. Earth Planet. Inter., 61: 269–290.

The source process of two large earthquakes that occurred in the Santa Cruz Islands subduction zone has been studied, one with a surface wave magnitude $M_s = 7.9$ in 1966 and the other with $M_s = 7.7$ in 1980. The seismic moment of the 1980 event estimated from long-period surface waves of Global Digital Seismograph Network (GDSN) and International Deployment of Accelerographs (IDA) records is 5.6×10^{27} dyn cm. Both of these events occurred at a shallow depth (i.e. between 20 and 40 km) with a similar thrust type focal mechanism with a strike ($\sim 347°$) parallel to the local trench axis, and they are located within 100 km in distance.

The 1966 event is a break of a single asperity which ruptured unilaterally to the north along the local trench strike and was truncated sharply at the northern boundary. This rupture pattern and the aftershock area expansion to the north indicate that there was a distinct barrier on the south of the 1966 source area. The major moment release of the 1980 event represents the rupture of this barrier. However, inversion of P-waves with an assumption of a constant focal mechanism failed to constrain the source process thereafter. In particular, the deconvolved source–time functions of the 1980 event do not show such a clear truncation as is observed in the 1966 source process, indicating that some unresolved features followed the peak of the moment release. Nevertheless, the 1-day aftershock area suggests that the rupture propagated to the north into the source area of the 1966 event.

We conclude that both earthquakes are subduction events between the Pacific and Indo-Australian plates; the 1966 event is a break of a single asperity and the 1980 event is a break of the remnant asperity which acted as a barrier for the 1966 source rupture. The subduction segmentation inferred from the intermediate-depth seismicity seems to control the mechanical condition of the subduction interface at shallow depths where the two large events took place. This interface created a barrier between the two source areas.

1. Introduction

The Santa Cruz Islands are located at the northernmost portion of the New Hebrides Island Arc, which is part of a complex boundary between the Pacific and the Indo-Australian plates (Fig. 1). Relatively smooth seafloor is being subducted in this area, but the bathymetric features of the overriding plate are complex. To the northwest of the Santa Cruz Islands, the Ontong–Java plateau is colliding with the Solomon Islands arc. To the north, a now inactive subduction zone, which consists of the North Solomon, Cape Johnson and Vitiaz trenches, subducted in the opposite direction to the currently active subduction zone. To the south of Vanuatu, the d'Entrecasteaux aseismic ridge is colliding with the New Hebrides Island arc and the subduction geometry is not clear in

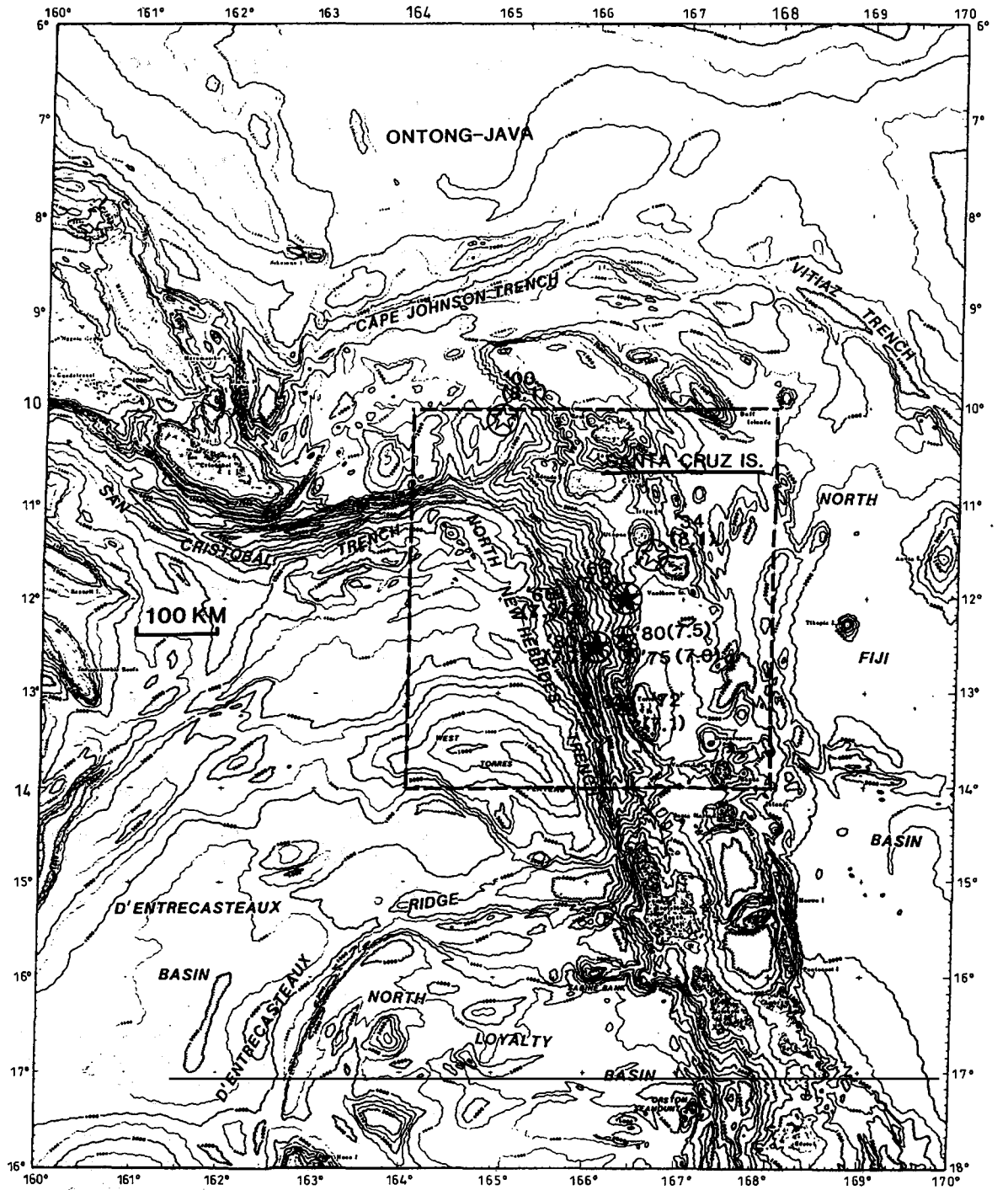

Fig. 1. Bathymetry map in the New Hebrides Island Arc and epicenters of major events which occurred in the study area (shown with a box) since 1900. The solid stars with a circle indicate the epicenters of the 1966, 1972, 1975 and 1980 events.

TABLE 1

List of large events

Year	Date		Time	Lat. (S)	Long. (E)	Depth	M_s (mbar)	
	Month	Day	h min s	(degrees)	(degrees)	(km)		
1966	12	31	18:23:8.8	11.9	166.4	73 40[a]	7.9 (5.5)	(main event)
			22:15:17.1	12.1	165.7	36	7.3 (5.2)	(aftershock)
1972	1	23	21:17:52.6	13.2	166.3	33	7.1 (5.8)	
1975	10	6	22:24:18.1	12.5	166.5	54	7.0 (6.0)	
1980	7	8	23:19:20.0	12.6	166.4	29	7.5 (5.9)	(foreshock)
	7	17	19:42:23.0	12.5	166.1	29[a] or 20[a]	7.7 (5.8)	(main event)

[a] Hypocentral depths used in the inversion.

this portion. Reflecting the tectonic conditions, the seismicity patterns are complex and the background activity is high (Malthelot, 1983; Wyss et al., 1983; Habermann, 1984). Moderate earthquakes ($M_s \sim 6$–7) occur frequently, but no large events with a magnitude of greater than 8.1 have been recorded since 1900. The spatial and temporal clustering of major events ($M \geq 7.0$) and the high level of background activity indicate the complex nature of asperity distribution in this region.

In the Santa Cruz Islands region, two large earthquake sequences, one with an $M_s = 7.9$ mainshock and the other one with $M_s = 7.7$, occurred in 1966 and 1980. Between these large earthquakes two moderate events ($M_s = 7.1$ and 7.0) occurred in this source area in 1972 and 1975 (see Table 1 and Fig. 1). The International Seismology Centre (ISC) location for the December 31, 1966 earthquake is 70 km east of the trench axis at 73-km depth. The hypocentral location and thrust type focal mechanism indicate that this earthquake is an interplate subduction event. The mainshock was followed by a large aftershock ($M_s = 7.3$) with an epicenter closer to the trench axis, after a few hours (see Table 1 and Fig. 1), and the aftershock area expanded mainly to the north for several months (Tajima and Kanamori, 1985). Because of this large earthquake sequence, the remnant high seismic potential which caused the 1980 event in the same area had not been properly assessed (McCann et al., 1979).

The 1980 sequence started with a large foreshock ($M_s = 7.5$) on July 8. The 1-day aftershock area of this event is located next to the southern boundary of the 1966 rupture area. The main event occurred within this area on July 17, with its epicenter being close to the trench axis. The epicenter location and the somewhat unexpected occurrence of the 1980 main event caused controversy as to whether this is an interplate subduction event or an intraplate one (Malthelot, 1983). However, our study shows that the focal mechanism of this earthquake is a thrust type with similar fault parameters to those of the 1966 main event. The aftershock area expanded to the north into the 1966 aftershock area for about 1 day and the activity level was low compared with the 1966 sequence. In view of the complex mechanical condition of subduction zone coupling, a simple concept of seismic gap or a simple recurrence law of large underthrusting earthquakes may not always explain the seismic activity in this area.

2. Body waveform inversion

2.1. Focal mechanisms and P waveforms

The focal mechanism of the 1980 main event is determined by the moment tensor inversion of Kanamori and Given (1981) using long-period surface waves recorded at the Global Digital Seismograph Network (GDSN; ANMO, ANTO, BOCO, CHTO, GUMO, BCAO, NWAO, GRFO, TATO, SNZO, CTAO, ZOBO, KAAO, MAJO, KONO) and International Deployment of Accelerographs (IDA;CMO, GAR, GUA, NNA, RAR, SEY, TWO, ESK, HAL, EIC) stations. The P-wave first motion data read from World Wide Standardized Seismograph Network (WWSSN) and

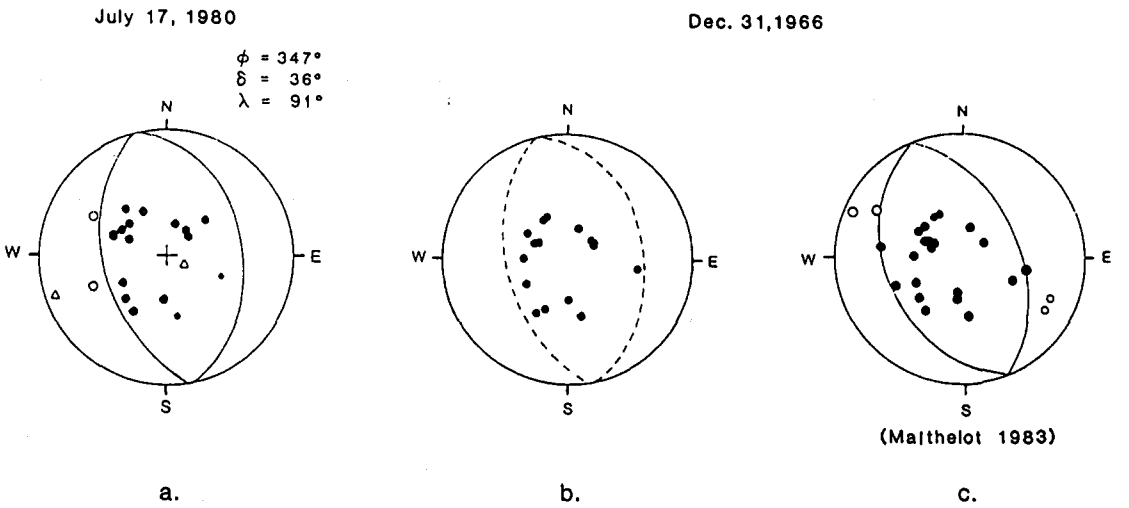

Fig. 2. (a) The focal mechanism solution of the July 17, 1980 event determined by a moment tensor inversion with GDSN and IDA records is shown on a lower hemisphere with an equal-area projection. The P-wave first motion arrivals read from WWSSN and GDSN records are also plotted. (b) The P-wave first motion arrivals of the December 31, 1966 event read from WWSSN records are plotted on the same focal sphere as that of the 1980 event. The nodal planes are shown with dashed lines. (c) The focal mechanism solution of the 1966 event determined by Malthelot (1983) using P-wave first motions read from WWSSN records and some local station records.

GDSN records are consistent with this solution (Fig. 2a). One of the nodal planes which both parallel the trench axis has a dip of 36° and a slip of 91° with a strike of 347°. These parameters are used as the fault solution.

The P-wave first motion data read from WWSSN seismograms do not constrain the nodal planes of the 1966 event, but are consistent with the solution of the 1980 event (Fig. 2b). This solution is also very similar to that of Malthelot (1983), who included readings of local station seismograms (Fig. 2c). Thus, we use the focal mechanism solution of the 1980 event to analyze the 1966 event as well. Although the focal mechanisms of these events are similar to each other, the P waveforms observed at stations common to the 1966 and 1980 events look different between the events. In Fig. 3 we compare P waveforms at stations, GDH, JCT, NNA, LPB, NAI, KEV and COL. The distribution of these stations has a satisfactory coverage of the azimuthal range. The records at COL are direct P-wave horizontal (north–south) components. All the other records are vertical components at distances between 100° and 128° from the epicenters. The waveforms are coherent from station to station for each event, but are different between the two events. The peak-to-peak amplitudes indicate that the two events are more or less comparable in magnitude, but the 1966 event is slightly larger than the 1980 event. The maximum peak-to-peak amplitude occurs earlier for the 1980 event than for the 1966 event. The waveforms of the 1966 event indicate a sharp rise and truncation of the source rupture process preceded by an introductory stage of minor energy release. On the other hand, the waveforms of the 1980 event do not show such a sharp truncation, but a strong pulse is followed by gradually attenuating complex waves.

2.2. *Methods of inversion*

To examine the source rupture process of these events, we apply two different body waveform inversion methods: the method of Ruff and Kanamori (1983) and that of Kikuchi and Fukao (1985). A brief description of the two methods is included in the Appendix. In essence, the method of Ruff and Kanamori (1983) determines the source–time history of a large event assuming a

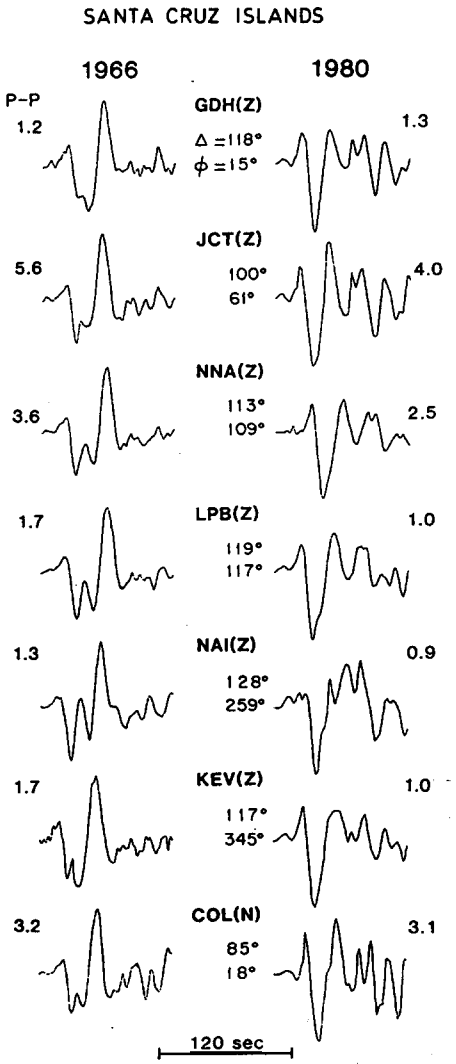

Fig. 3. P-wave forms of the 1966 and 1980 events observed at seven common stations. The records at COL are horizontal components (north) and all the others are vertical ones. The coherency of waveforms of each event among the stations and the difference between the stations are noteworthy. The peak-to-peak amplitudes (cm) are indicated.

Green's function for a double-couple source that is constant with time. A one-dimensional spatial map of the moment release can also be determined by using the directivity effect in the deconvolved source–time functions among different station azimuths. The advantage of this method is the applicability to diffracted P-waves to extract gross features of a rupture process. As many of the vertical component records of the direct P-waves of the Santa Cruz Islands events are off-scale and unusable for the analysis, we first use this method including diffracted P-waves recorded on the vertical component and direct P-waves obtained from horizontal components.

The iterative two-dimensional (2-D) inversion method of Kikuchi and Fukao (1985) models an earthquake source as a series of double-couple point sources which are specified by the coordinates (x, y) on a given fault plane, the seismic moment (m) and the onset time (t). Here, the inversion scheme includes the directivity effect among the stations and determines a series of double-couple point sources (m_i, t_i, x_i, y_i, $i = 1$, n) using the same algorithm as was described by Kikuchi and Kanamori (1982). This inversion scheme implies that no restriction is applied to the spatial and temporal pattern of rupture propagation on a given fault. Although only direct P-waves are usable for this inversion, the method of Kikuchi and Fukao (1985) can determine the source–time function and the point source distribution on a given fault plane simultaneously.

The common assumption of these methods is that the focal mechanism stays constant during the rupture process. When this assumption is valid, the main features of the rupture process should be consistent between the two methods.

2.3. *Results*

1966 Main event

A source depth of 73 km is listed in the ISC catalogue for this event. However, the time function deconvolved for this depth with the method of Ruff and Kanamori (1983) shows spurious quasi-harmonic oscillations throughout the duration of the time function (see Fig. 4). This type of oscillation is commonly observed when the source depth is overestimated (Christensen and Ruff, 1985). The time functions deconvolved from the record at NNA for different depths and the synthetic waveforms corresponding to the observed ones are shown in Fig. 4. We performed a similar test for three other stations (ATL, LPS and KEV) and found that the time function is most stable (impulsive) for a depth between 30 and 40 km. In

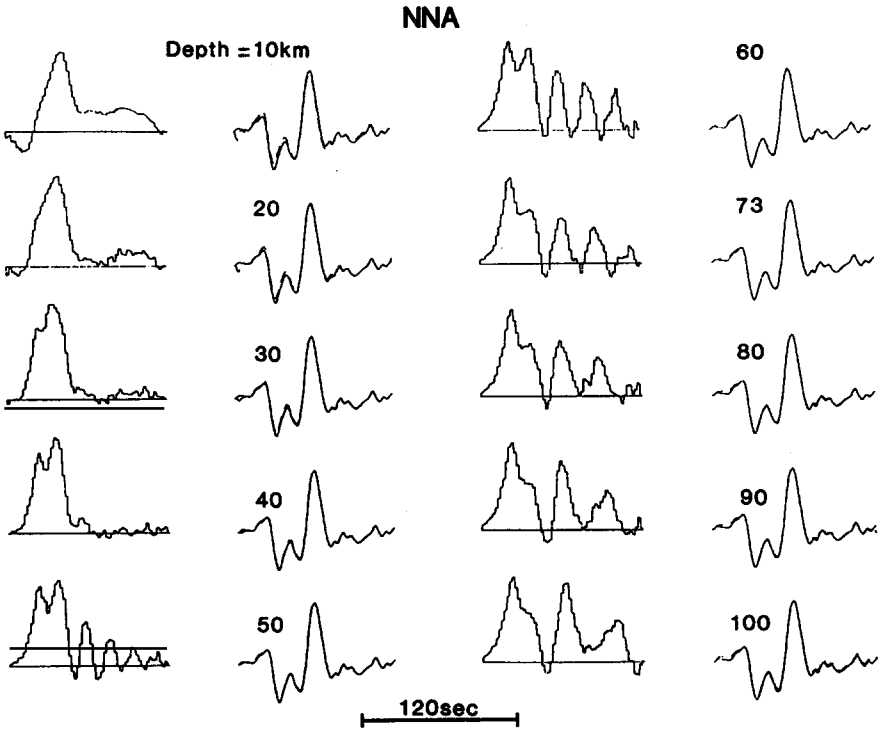

Fig. 4. Deconvolved station–time functions from the 1966 event record observed at NNA for various point source depths. The time function deconvolved for the ISC depth of 73 km shows oscillations. This figure indicates that a depth of 40 km is most adequate for the point source of this event.

the following analysis we use 40 km for the source depth of the 1966 event.

In Fig. 5 we show the source–time functions deconvolved from 19 stations and the corresponding observed and synthetic waveforms. Direct P waveforms ($\Delta < 103°$) are used only at five stations, BAG, SPA, JCT, GOL and COL. The waveforms for BAG and COL are converted from the horizontal (east–west and north–south) components to vertical ones using the formula given by Bullen (1953). The time functions are coherent among the stations and show a clear rise and two truncations. The sharp rise is preceded by an introductory rupture with a small amount of energy release. The duration time of the introductory rupture, which we denote by t_0, is measured to be 8–14 s depending on the azimuthal locations of the stations. The first truncation overlaps the initiation of the second rise, which is followed by a sharp truncation. The first and second truncation times measured from the onset time are denoted by t_1 and t_2, respectively. Following Beck and Ruff (1984), we investigated the rupture pattern of the source by examining the directivity of t_0, t_1 and t_2. We assume that these correspond to the arrival times of P-waves radiated from distinct features in space and time. That is, if a distinct feature occurs at a distance X from the epicenter, along the azimuth θ_0, at time t, then the arrival time of the corresponding P-wave at the ith station relative to the first motion is given by

$$t_i = -p_i \cos(\theta_i - \theta_0) X + t \qquad (1)$$

where p_i is the ray parameter for the station and θ_i is the azimuth of the station. We call $\gamma_i = p_i \cos(\theta_i - \theta_0)$ the directivity parameter. X, t and θ_0 are determined so that the observed and computed t_i are best correlated. The rupture direction of the event corresponding to the second truncation t_2 is determined to be N30°W with a correlation coefficient of 0.81 (Fig. 6a). The directivity between the first and second truncations ($t_2 - t_1$)

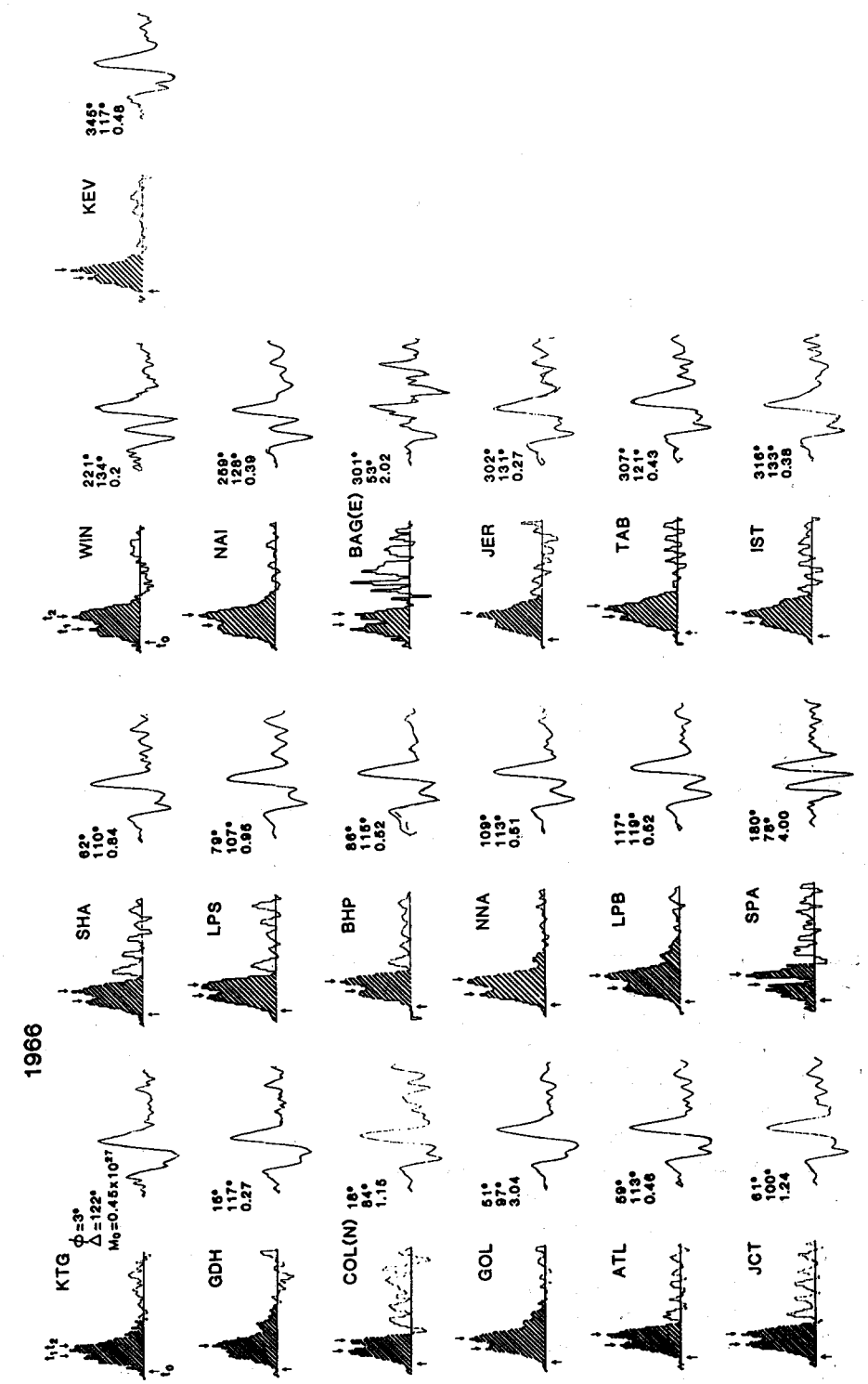

Fig. 5. Station–time functions of the 1966 event deconvolved from 19 stations. The records at COL and BAG were converted from the horizontal components to vertical ones. It should be noted that a sharp rise and two comparable sharp truncations (denoted by t_0, t_1 and t_2) are commonly observed at most of the stations.

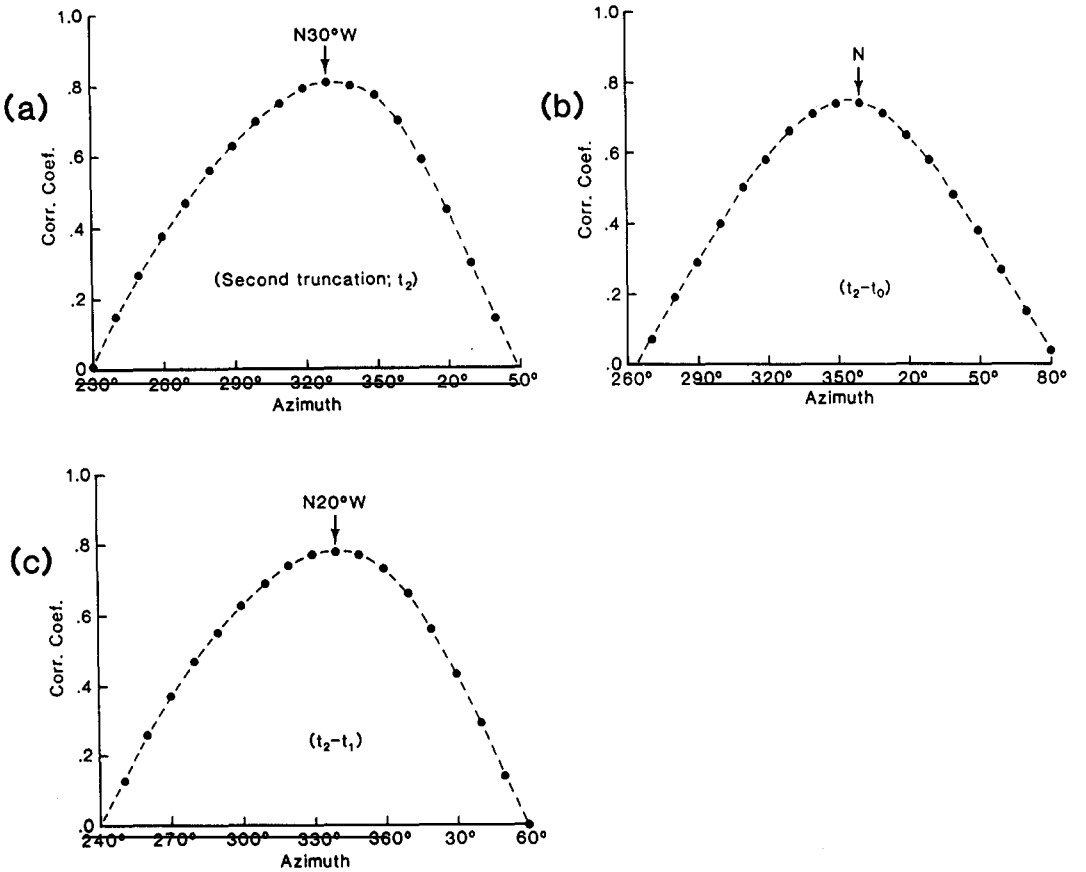

Fig. 6. Correlation coefficients calculated between the directivity parameter (see the text for the definition) and time t_2, $t_{12} = t_2 - t_1$ and $t_{02} = t_2 - t_0$ measured in the deconvolved time functions of the 1966 event as a function of rupture direction. These diagrams indicate that (a) the second truncation t_2 occurred in the direction N30° W from the epicenter; (b) the second truncation occurred in the north from the initiation of the major rupture at t_0; and (c) the second truncation occurred in the direction N20° W from the first one.

is also clear, with a correlation coefficient of 0.78 for the rupture direction N20° W (Fig. 6c). The duration time of the introductory rupture measured at t_0 or the first truncation at t_1 in relation to the epicenter does not show clear directivity. However, the second truncation time measured from the initiation of the first rise, i.e. $t_2 - t_0$ shows directivity with a correlation coefficient of 0.74 for the rupture direction north (Fig. 6b). The rupture directions north to N30° W are close to the fault strike of this event. Figure 7a shows the plots of the episodic arrival times, e.g. t_2, $(t_2 - t_1)$ and $(t_2 - t_0)$ versus the directivity parameter for the rupture directions N30° W, N20° W and north, respectively. From this plot we determined that the second truncation occurred at 47.5 ± 8.5 km N30° W from the epicenter, at $t_2 = 35.8 \pm 1.2$ s after the initiation of the rupture. The distance between the first and second truncations is 34.3 ± 6.7 km, and the time interval is 10.6 ± 1.0 s (Fig. 7a). In Fig. 7b we illustrate the rupture pattern inferred from the directivity analysis. Here, E denotes the epicenter and R_0, R_1 and R_2 show the locations of the features which are measured teleseismically at t_0, t_1 and t_2. The solid lines and the arrow indicate the rupture propagation, and the dashed lines the relative locations of the second truncation to the epicenter and the starting point of the major rupture. Locations E, R_0 and R_1 are within a diameter of 25 km. Because of this small

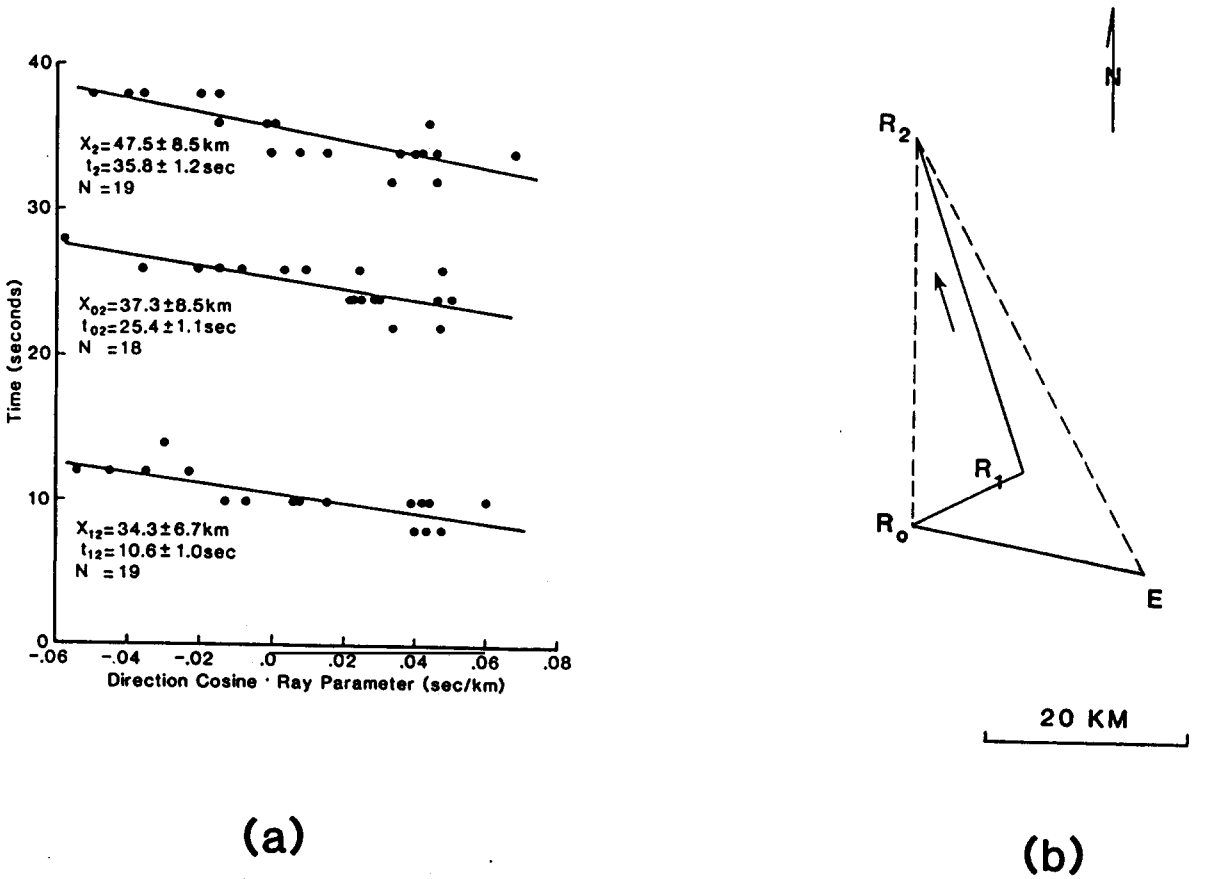

Fig. 7. (a) The time, t_2, t_{12} and t_{02} vs. directivity parameter (direction cosine times ray parameter) are plotted for the most adequate relative directions. (b) Rupture propagation inferred from the directivity analysis is shown with solid lines.

dimension, we did not observe any directivity effect for these features. Time t_1 is estimated to be ~ 25 s, and accordingly the apparent rupture velocity of this stage is slow. It seems that the rupture between E and R_1 started the major rupture, and probably developed the full width of the fault. After this, the rupture propagated relatively fast, with an apparent rupture velocity of 3.3 ± 0.9 km s^{-1} between R_1 and R_2, which are 34.3 ± 6.7 km apart. We should consider that the point R_2 represents the truncation of the fault rupture with a finite width. The linear feature of the rupture extracted from the directivity effect indicates that the rupture propagated continuously northward. Therefore, the source process of the 1966 event is a unilateral rupture of a single asperity.

With the 2-D inversion method of Kikuchi and Fukao (1985), we obtained a similar result to that with Ruff and Kanamori's method in terms of source–time history and rupture propagation direction. Here we used only records obtained at stations within 110° from the epicenter. First, we checked the sensitivity and stability of the inversion by changing the hypocentral depth, τ_1 and τ_2 (see Appendix for the definitions of the parameters). In general, when the depth is not chosen properly, the deconvolution is unstable, i.e. the resultant spatial and temporal patterns of the source process vary for different combinations of τ_1 and τ_2. In this sense, the deconvolved source–time history of the 1966 event is most stable for a source depth of 40 km, which is consistent with

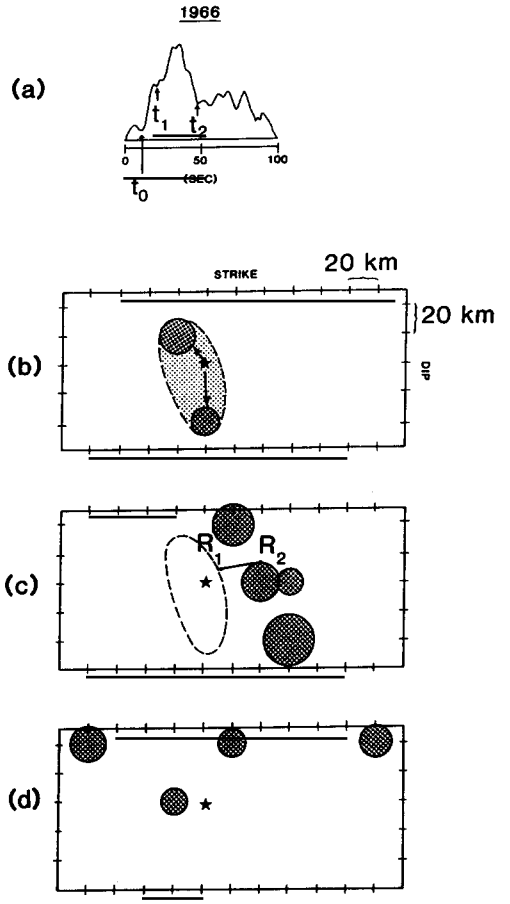

Fig. 8. (a) Source–time function determined for the 1966 Santa Cruz Islands earthquake. The source depth is 40 km and, τ_1 and τ_2 are 5 and 10 s, respectively. The normalized error is 0.297. The episodic times t_0, t_1 and t_2 determined by the directivity effect (see Fig. 7a) are also indicated. (b) Spatial distribution of point sources for the period $0 \leq t \leq 12$ s. The radius of circles is proportional to the seismic moment of individual sources. The solid star shows the epicenter. (c) Same as (b) for the period $12 < t \leq 31$ s. The locations R_1 and R_2 (see Fig. 7b) are indicated. (d) Same as (b) for the period $31 < t \leq 100$ s. The dashed line indicates the source area.

the result by Ruff and Kanamori's method. The normalized error gives a minimum value of 0.297 for the combination $(\tau_1, \tau_2) = (5, 10)$. Figure 8a shows the corresponding source–time function in which t_0 t_1 and t_2 determined by Ruff and Kanamori's method are marked. The features observed at t_0, t_1 and t_2 are also clearly identified in this source–time function. Figures 8b, c and d illustrate the spatial pattern of the rupture process with the deconvolved point sources for different time intervals. In each of these figures the coordinates are chosen along the strike ($\phi = 347°$) and dip ($\delta = 36°$) with a grid interval of 20 km. Each point source is shown with a circle which is proportional to the magnitude. Figure 8b shows that the introductory rupture propagated bilaterally to the east and west until the fault width became ~ 80 km at 12 s after its initiation. This stage is described for the period up to t_1 in the source–time function (Fig. 8a). Then, the rupture of major energy release started. This stage is described between t_1 and t_2 in Fig. 8a. All the point sources deconvolved during this period are located to the north of the epicenter (Fig. 8c). This pattern suggests that the rupture propagated to the north along the fault strike and was truncated at a distinct boundary; the source process is interpreted as a single unilateral rupture. After this stage, the point source locations are widely spread along the strike at shallow depths (e.g. $h \simeq 0$ km, Fig. 8d). In Fig. 8c we also illustrate the locations R_1 and R_2 indicated in Fig. 7b. These locations are approximately in the middle of the fault width determined by the 2-D inversion. The synthetic waveforms for this source–time function are compared with the observed ones in Fig. 9. At stations PEL, SPA and BAG there are some differences between the observed and synthetic waveforms. Otherwise the agreement is satisfactory.

1980 Main event

After we examined time functions for several different depths using Ruff and Kanamori's method, we determined that the source depth of 29 km listed for the 1980 main event in the ISC catalogue is adequate. This suggests that the depth interval over which most of the moment release occurs is nearly the same for the 1966 and 1980 main events. The deconvolved source–time functions and the corresponding synthetic and observed seismograms are shown in Fig. 10. Again, because of saturation, the direct P-wave vertical component ($< 103°$) is usable only at six stations (GUA, RAR, KIP, LON, NDI and LUB). The records obtained at stations near the node on the focal sphere (MUN, TAU) or contaminated for some reason were omitted. The records at COL,

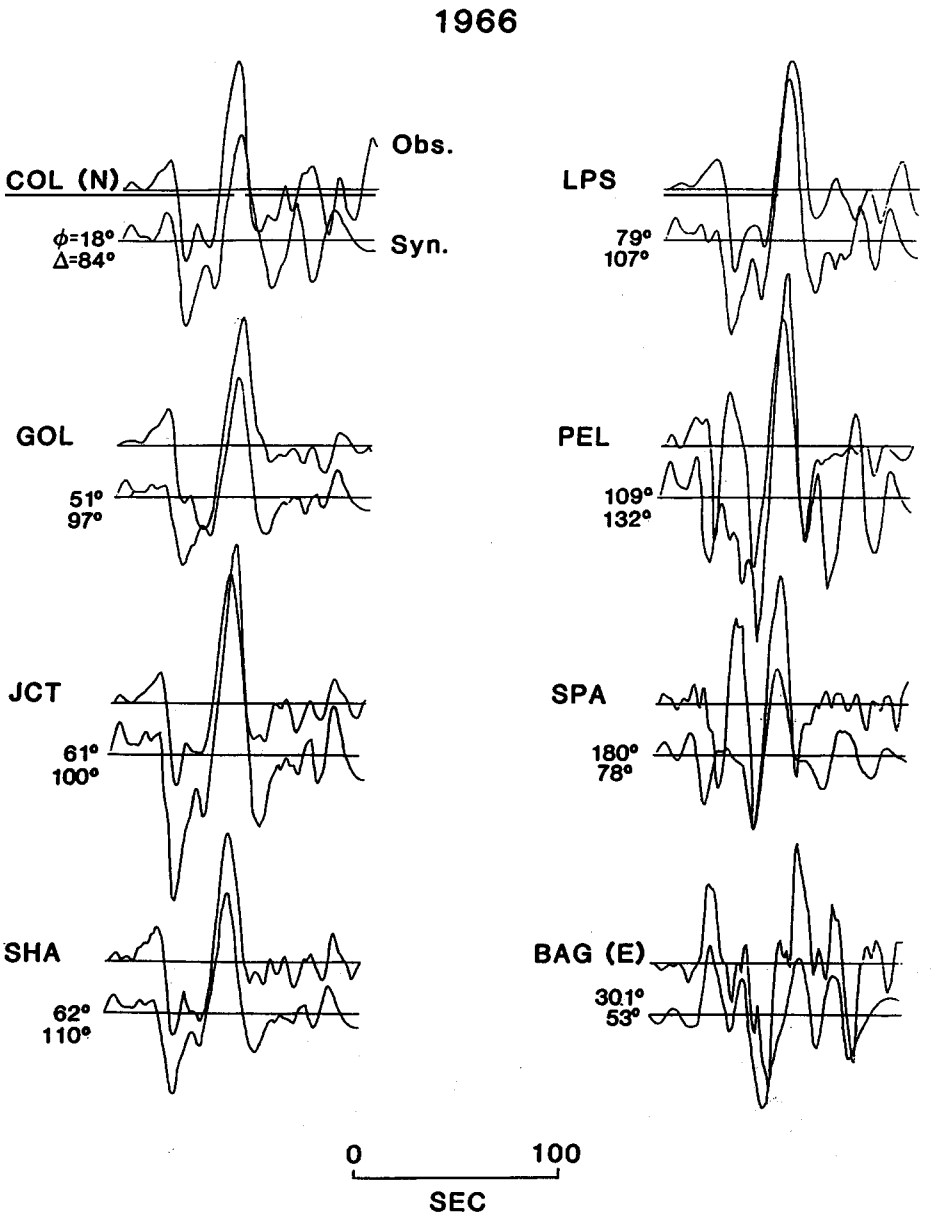

Fig. 9. Comparison of synthetic waveforms made with the source–time function in Fig. 10 with observed waveforms.

ANP, SHK, GSC, SBA and DUG were converted from a horizontal component and show more high-frequency noise. The time functions deconvolved from diffracted P-waves at stations, NNA, LPB, UME and KEV are relatively smooth and similar to each other, indicating that the energy release peaked at ~ 30 s after the initiation, then decreased gradually and was complete within 30 s afterwards. Those of the other diffracted P-waves such as GDH, FVM, GIE, ANT, LPA, NAI and KBS appear to show some subevents after the peak of the energy release. Those which were deconvolved from direct P-waves, i.e. at stations RAR, KIP, GUA and LON show more high-

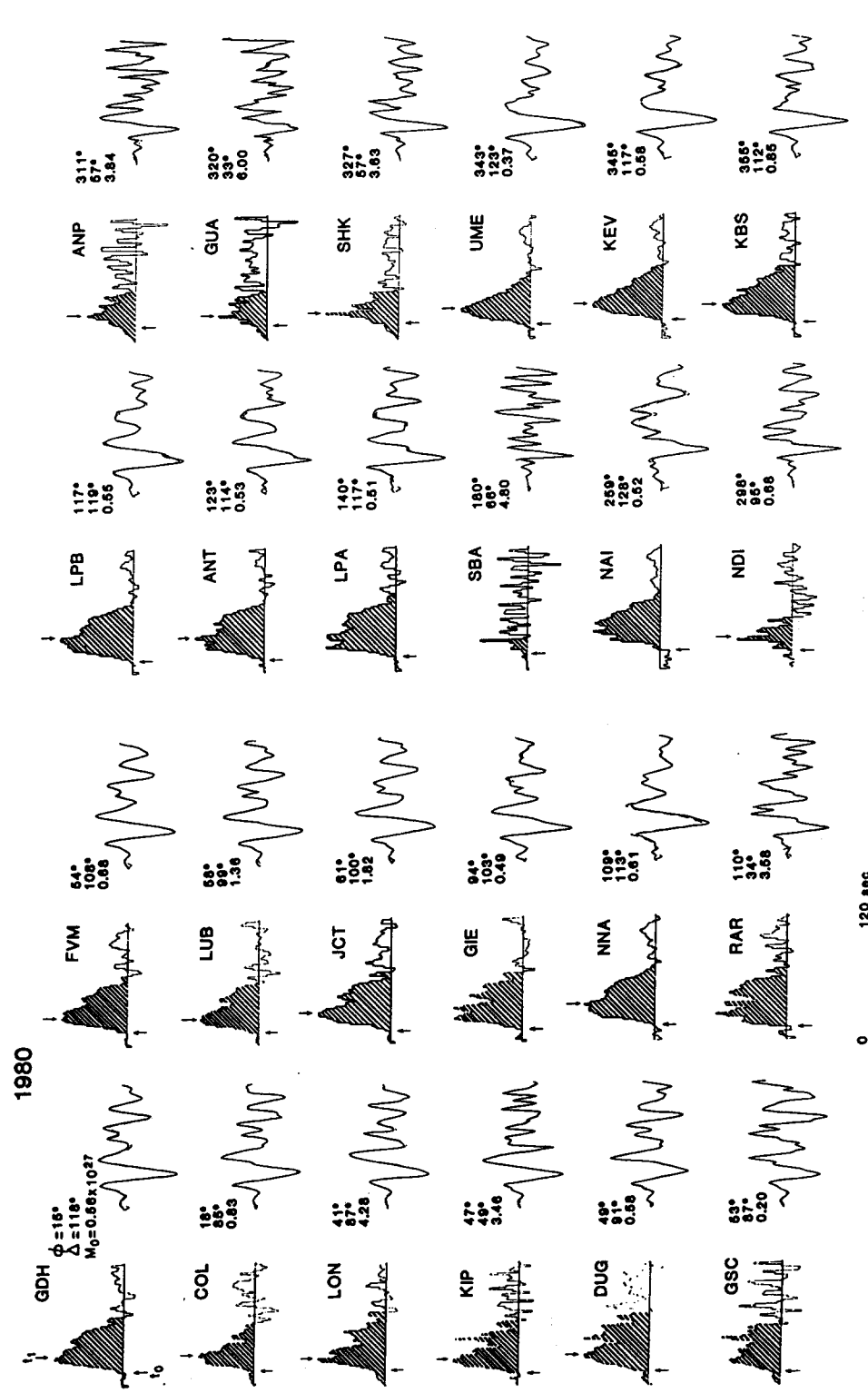

Fig. 10. Station–time functions of the 1980 event deconvolved from 24 station records. Those deconvolved from diffracted P waveforms such as at LPB, NNA, KEV, UME, GDH and FVM are relatively smooth. Time functions deconvolved from direct P waveforms such as at KIP, GUA, LON and others appear to be more complex. A truncation of the major energy release at t_1 is commonly observed in many time functions but it is not as sharp as was observed in the time functions of the 1966 event. An introductory rupture with duration of t_0 preceded the major energy release.

frequency details. In general, the major energy release was preceded by a minor precursory rupture with a duration of 12–18 s, denoted as t_0, which was measured at 19 stations. The highest correlation coefficient between the directivity parameter and t_0 is 0.72 for the rupture direction N80°E; the rupture propagation is 36.4 ± 5.7 km for 14.7 ± 1 s. This implies that the main rupture episode actually started at the down-dip edge of the ruptured area; the listed location is merely a foreshock or precursory rupture (the same situation is obtained for the 1969 Kurile Islands earthquake; Schwartz and Ruff, 1985). However, the energy release during this stage is very small and the correlation coefficient of 0.72 does not indicate a strong directivity.

This precursory stage was followed by the rupture with major energy release which was truncated at time t_1. This truncation is, however, not as sharp as that observed in the source process of the 1966 event, and is ambiguous at some stations (e.g. GIE, RAR, LPA and NAI). The moment release then decreases, with ~ 30-s duration apparently composed of a few smaller subevents. For this source process the event association is more difficult, as the details of the source–time function vary between different stations. Indeed, the highest correlation coefficient for t_1 is just 0.63 for a direction of N10°W. Ruff and Kanamori's method does not seem to distinguish effectively the moment release peak or other distinct features of this particular source process. In an attempt to distinguish further the spatial location of moment release, we applied Kikuchi and Fukao's method (1985) for potentially higher resolution.

We have performed a similar test for the data set of the 1980 event, changing the source depth and the combination of τ_1 and τ_2. For a source depth of 29 km the deconvolution was unstable, i.e. the spatial and temporal pattern of the deconvolved source process changed substantially for different combinations of τ_1 and τ_2. For a hypocentral depth of 20 km the result was relatively stable with a minimum normalized error of 0.308 if the combination of parameters $(\tau_1, \tau_2) = (6, 9)$. As is shown in Fig. 11a, two subevents are distinguished in the source–time function. Although

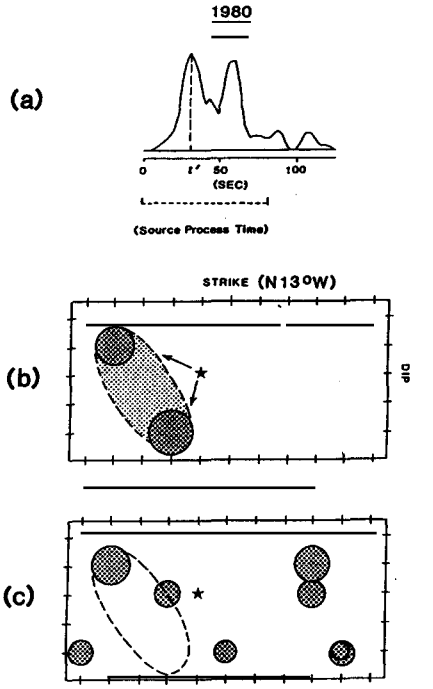

Fig. 11. (a) Source–time function determined for the 1980 Santa Cruz Islands earthquake. The source depth is 20 km, and τ_1 and τ_2 are 6 and 9 s respectively. The normalized error is 0.308. The dotted line under the source–time function indicates the source–process time measured from the spectra of the long-period surfaces waves of GDSN records at 250 s. (b) Same as Fig. 8(b) for the 1980 event for the period $0 \leq t \leq 30$ s. (c) Same as (b) for the period $30 < t \leq 82$ s.

we observe subevents in the down-ramp in some of the source–time functions in Fig. 10, they are not as obvious as in Fig. 11a. The dotted line under the source–time function indicates the source–process time (Furumoto, 1979; Furumoto and Nakanishi, 1983) to be 82 s measured from long-period surface wave spectra of GDSN records at 250 s. The source–process time is very similar to the duration time of the major moment release in Fig. 11a. Figures 11b and c show the spatial point source distributions determined for two different periods which are divided at $t' = 30$ s. The first major moment release is located to the south and east of the epicenter (Fig. 11b). This stage corresponds to the first sharp rise before t' in the source–time function (Fig. 11a).

The point source locations determined for the period between t' and 82 s are shown in Fig. 11c.

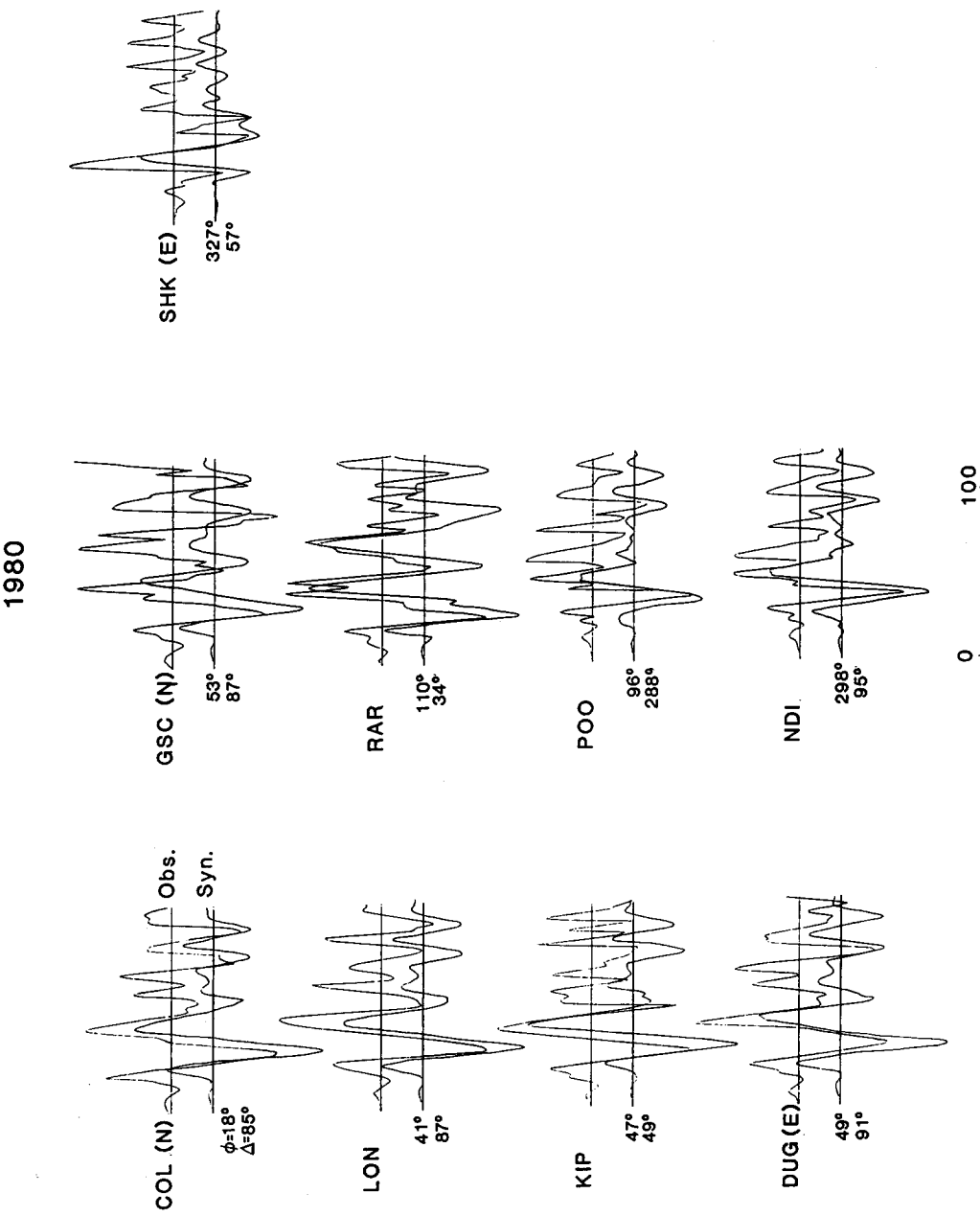

Fig. 12. Comparison of synthetic waveforms made with the source–time functions in Fig. 11(a) with observed waveforms.

During this stage we do not see any coherent pattern of point source distribution and therefore cannot constrain the rupture pattern. Although we were not able to resolve any further pattern of major moment release even by the 2-D inversion method, our important finding is that the primary location of major moment release lies to the southeast of the epicenter, near the southern boundary of the 1966 source area. The agreement between the synthetic waveforms for the source–time function (Fig. 11a) and the observed ones is satisfactory within 50 s after the onset but not for the later part (Fig. 12).

The results of P waveform inversions of the 1966 and 1980 Santa Cruz Islands main events suggest that the source processes are clearly different from each other, although these two large events have a very similar focal mechanism and magnitude to each other, and occur in the same subduction zone at shallow depths. The 1966 source process is a typical subduction event; it is a break of a single asperity with its rupture propagating to the north unilaterally. The main event rupture pattern indicates that there is a distinct boundary which remained unbroken during this event around the southern boundary of the source area. For the 1980 earthquake, this barrier ruptured at an early stage of the source process and was located around the southern boundary of the 1966 source area. Otherwise, our body waveform inversions failed to constrain the entire source process of this event.

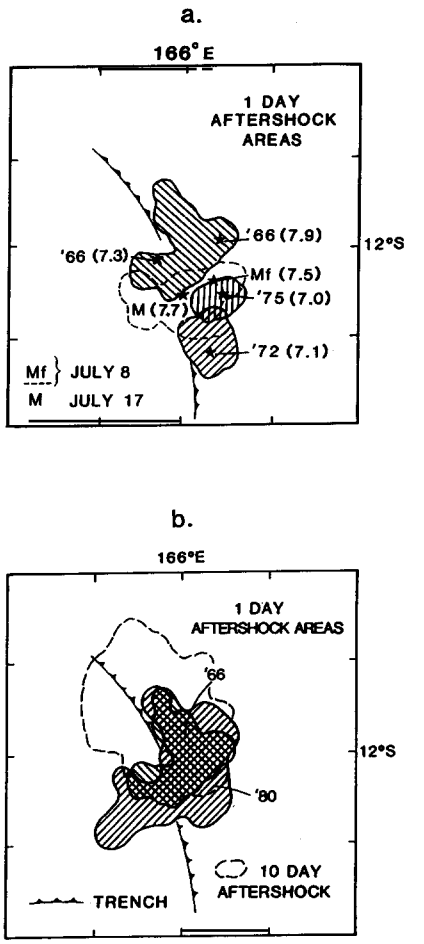

Fig. 13. (a) The 1-day aftershock areas of the 1966, 1972 and 1975 sequences determined by the energy-contour map method (Tajima and Kanamori, 1985) are shown by shading. That of the July 8 foreshock of the 1980 sequence is indicated by dots. The epicenters of the mainshocks, the largest 1966 aftershock and the July 8 foreshock are shown with solid stars. (b) The 1-day aftershock areas of the 1966 and 1980 sequences. The dotted line indicates the 10-day aftershock area of the 1966 event. The 1980 main event sequence started on July 17; the aftershock area heavily overlapped that of the 1966 event.

3. Seismicity and subduction zone geometry

3.1. Aftershock distribution of the 1966 and 1980 sequences

Figure 13 shows the aftershock areas of the 1966 and 1980 earthquakes and some other major events based on the study by Tajima and Kanamori (1985). The 1966 main event was followed by a large aftershock ($M_s = 7.3$) in 4 h (see Table 1). The southwestern portion of the 1-day aftershock area corresponds to this activity. The aftershock area expanded mainly to the north along the trench strike during a 10-day period; the expansion to the south is slight. This pattern is consistent with the main event source process.

The 1980 earthquake sequence started with a large foreshock (M_f) which created the 1-day aftershock area (shown with a dotted line in Fig. 13a) next to the southern boundary of the 1966 1-day aftershock area. The source areas of the two moderate events in 1972 and 1975 also overlap the

1-day aftershock area of this event (M_f) (Fig. 13a). The 2-D inversion determined that the major energy of the 1980 main event was also released within the 'aftershock area' of the foreshock. The 1-day aftershock area of the 1980 main event includes that of the 1966 event (Fig. 13c). Although the P-wave inversions failed to determine the rupture process thereafter, this aftershock distribution indicates that the rupture propagated to the north into the 1966 1-day aftershock area. After 1 day, the aftershock area expanded very little. These observations suggest that there was a distinct barrier at the southern boundary of the 1966 source area and that this barrier prevented the rupture propagation of the 1966 event to the south. In this context, the 1980 event is a break of the remnant asperity which acted as the barrier for the 1966 event.

3.2. *Plate segmentation and fault zone heterogeneity*

Based on the results shown above, we illustrate the asperities estimated for the 1966 and 1980 main source ruptures on the bathymetry map (Fig. 14). Points R_1 and R_2 correspond to those in Fig. 7b. The stars show the mainshock epicenters. The dimension of the asperity for the 1966 event is estimated by the results of P-wave inversions and the 1-day aftershock area. The rupture started near the southeastern boundary of the asperity and propagated to the north along the trench axis. The truncation of the rupture was clearly identified at point R_2 as this source process was interpreted as a rupture of a single asperity. The asperity for the 1980 event is around the southern boundary of the 1966 aftershock area.

The different source characteristics observed

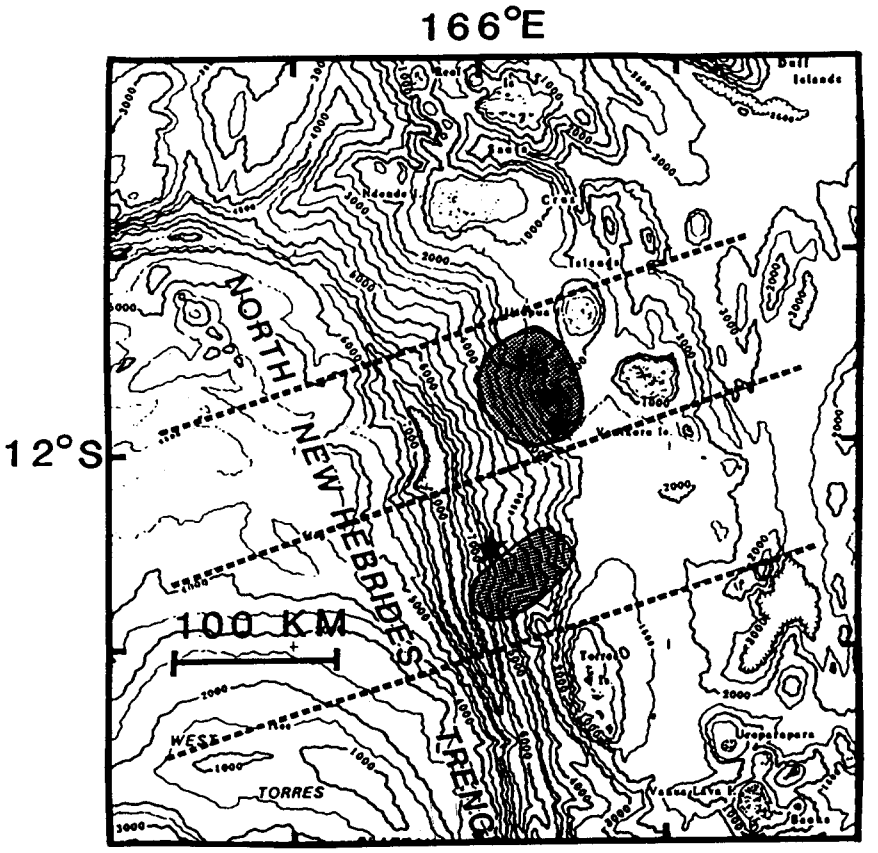

Fig. 14. The asperity distributions inferred from the inversions and the mainshock epicenters are illustrated on the local bathymetry map.

from the 1966 and 1980 main events reflect the different conditions of coupling between the descending slab and the overriding plate in this subduction zone. Although the aftershock zones expanded into adjacent rupture zones, we can still recognize a major seismic segmentation boundary between the 1966 and 1980 mainshock source areas. Whatever the physical realization of this boundary is, it apparently has a substantial extension in the deeper Benioff zone.

From this point of view, we examine the spatial seismicity pattern in this subduction zone (10–14°S; 164–168°E) for the period from 1964 to 1981 using the ISC catalogue. Figures 15a–d show the spatial seismicity patterns for depth ranges between 0 and 70 km, 70 and 160 km, 160 and 250 km and > 250 km, respectively. In the depth ranges of $0 \leq h \leq 70$ km and $70 < h \leq 160$ km the seismicity patterns do not show great variation along the trench axis. In the range between 160 and 250 km the seismic activity for the subduction zone of the 1980 source area is substantially higher than that of the 1966 source area. Deeper than 250 km, only the portion below the 1980 source area shows activity. In the subduction segment where deep seismic activity is clearly deficient, we observe volcanic activity on the surface (see Fig. 14). To examine the subduction geometry more clearly, we project events in the cross-sections indicated with (1) and (2) in Fig. 15d. These cross-sections correspond to the subduction zones of the 1966 and 1980 source areas. The pole of the projection is sufficiently far from the trench axis for each cross-section to describe the local subduction

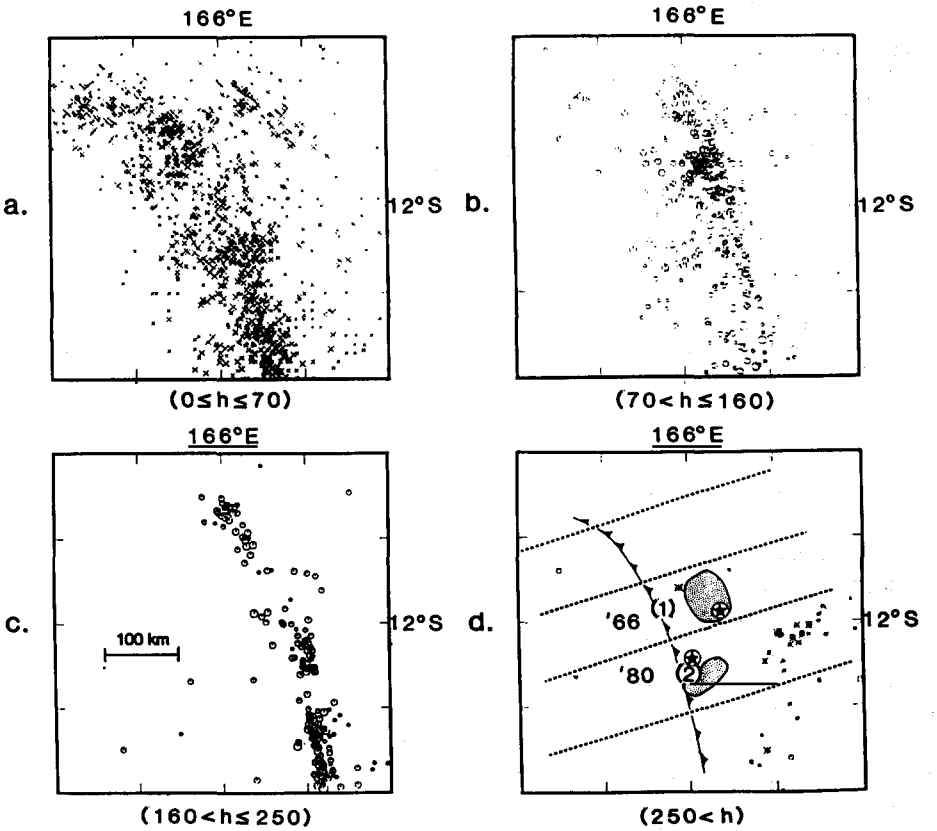

Fig. 15. Spatial seismicity patterns in different depth ranges during the period 1964–1981 based on the ISC catalogue. (a) $0 \leq h \leq 70$ km. (b) $70 < h \leq 160$ km. (c) $160 < h \leq 250$ km. (d) 250 km $< h$. The subduction segments are divided by the dotted lines which indicate the cross-projections in Fig. 16. The asperity distributions in Fig. 14 are also shown.

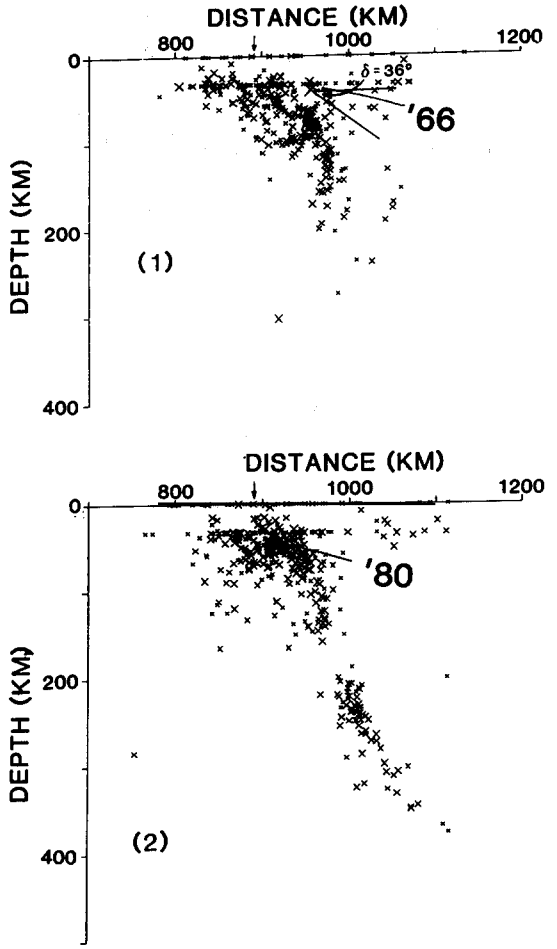

Fig. 16. Cross-projection of subduction geometry in the segments marked as (1), and (2) in Fig. 15(d). The data base is the same as in Fig. 15.

geometry properly. Figure 16 shows the results, In cross-section (1) events are observed mostly at depths shallower than 200 km. The revised hypocenter of the 1966 main event is indicated. In zone (2) the subduction zone seismicity extends to a depth of 400 km. The hypocentral location and the dip angle of the fault solution of the 1980 main rupture are indicated. The events deeper than 200 km define an almost straight descending slab. This fault geometry suggests the effects of unbending forces at intermediate depths (Kawakatsu, 1986). From these observations we propose that there must be a distinct interface between the two segments (1) and (2); this interface created a barrier which blocked the 1966 main source rupture and, this barrier was the source of the major energy release of the 1980 event. Thus, the seismic segmentation between the 1966 and 1980 source areas is correlated to different behavior in the deeper Wadati–Benioff zone.

4. Discussion and conclusion

Using the source parameters obtained above, we attempt to assess the average stress drop $\Delta\bar{\sigma}$ and the seismic slip $\overline{D}$ of the 1966 earthquake according to the formulae of Kanamori and Anderson (1975):

$$\Delta\bar{\sigma} = \frac{8\mathrm{Mo}}{3\pi LW^2} \tag{2}$$

$$\Delta\overline{D} = \frac{\mathrm{Mo}}{\mu S} \tag{3}$$

where Mo is the released seismic moment, L and W are the fault length and width, S is the fault area and μ is the rigidity 5×10^{11} dyn cm^{-1}. Although the long-period surface wave moment is not available for the 1966 event, that for the 1980 event calculated from GDSN and IDA records is 5.6×10^{27} dyn cm. The comparison of the peak-to-peak amplitudes of body waves at the common stations (see Fig. 3) suggests that the moment of the 1966 event is comparable to that of the 1980 event. On the other hand, in reality, the assessment of the source area is not straightforward, as we observed a discrepancy of source dimension determined between the 2-D inversion and the aftershock area. If we adopt a source dimension determined by both the 2-D inversion and the 1-day aftershock area, e.g. $W = 80$ km and $L = 70$ km, the stress drop is 11 bar and the seismic slip 200 cm for the 1966 event. Adopting a relative tectonic slip rate in this subduction zone of 10.9 cm a^{-1} (Minster and Jordan, 1980), the accumulated tectonic slip is 349 cm since the previous large event in 1934. The ratio of seismic slip to the accumulated tectonic slip (Kanamori, 1977) then is 0.57 for this event.

The northern part of the 1980 aftershock area is located in the aftershock area of the 1966 event, and therefore estimation of the accumulated

tectonic stress for this source area is not easy. Although we were not able to constrain the source dimension by the P-wave inversions, the 1-day aftershock area appears to be substantially larger than that of the 1966 event. If we assume that the 1-day aftershock area represents the source dimension, the source area of the 1980 event is about twice as large as that of the 1966 event and the seismic slip rate is about half that of the 1966 event. This assumption supports the hypothesis that the average strength of seismic coupling of this source area was relatively weak because of a short recurrence interval, and accordingly, the average stress drop is lower when two earthquakes are comparable in moment release to each other. As mentioned above, the seismic slip rates are usually estimated with substantial uncertainties depending on the determination of the source dimension. However, the values suggested for the Santa Cruz Islands region have a similar range to those obtained for subduction zones such as in the Aleutians or the Kuriles (Kanamori, 1977; Sykes and Quittmeyer, 1981; Peterson and Seno, 1984).

After the barrier broke, the 1980 source process has not been resolved clearly. We address two possible reasons, e.g., either (1) the rupture continuously propagated to the north into the 1966 source area, as indicated by the 1-day aftershock area, or (2) the apparent long-lasting source process could be the effects of water reverberations (Wiens, 1989). In case (1) the seismic coupling in the northern part was weak before the event. Accordingly, the source process in the northern part is essentially a reactivation of existing faults which had been created during the 1966 sequence and produced different slips from that determined for the 1980 mainshock with the surface wave moment tensor and P-wave first motions (Tajima and Célérier, 1989). Case (2), which is not as easy to test in a unique sense, is a possibility, as the epicenter location of the 1980 event is closer to the trench axis than is that of the 1966 epicenter. The water depth above it is deeper than that for the 1966 epicenter. This situation could cause strong effects of water reverberation on the P waveforms (Wiens, personal communication).

McCann et al. (1979) assumed that the seismic potential of the 1980 source area was low since the 1966, 1972 and 1975 earthquakes and that the aftershocks had filled the region already. As we examined the source area of the 1966 event by both P-wave inversions and seismicity, an area with remnant seismic potential was found around the southern boundary of the rupture zone. The 1972 and 1975 events are moderate, and were apparently not large enough to release that seismic potential. This study suggests that complete source process study combined with seismicity is required to assess properly a remnant high seismic potential, particularly in complex subduction zones.

The results of our study showed the similarities and differences of the source characteristics of the 1966 and 1980 Santa Cruz Islands earthquakes. The revised source depth of the 1966 event ($\sim$ 40 km) is shallower than that listed in the ISC catalogue, and thus both earthquakes are shallow large events with a similar underthrusting focal mechanism and comparable moment release. We conclude that both events represent subduction of the Indo-Australian plate beneath the Pacific plate. The 1966 event is a break of a single asperity which ruptured unilaterally to the north and was sharply truncated. This pattern indicated that there was a distinct barrier on the south of the 1966 source area, which blocked the rupture propagation and the aftershock area expansion to the south. The two moderate events in 1972 and 1975 and the July 8, 1980 foreshock all occurred around this barrier. The major moment release of the 1980 event represents the rupture of this barrier.

The segmentation of the shallow seismogenic zone is correlated with a variation in the deeper part of the subduction geometry. The subduction zone for the 1980 event extends to a depth of $\sim$ 400 km (zone (2) in Fig. 16) whereas that for the 1966 event extends to 200 km. Eventually, the effective force for the 1966 event was caused by the 'subduction push' and that for the 1980 event was caused by the 'subduction pull'. Of course, we cannot uniquely determine whether some lateral physical variation in the downgoing slab causes both the seismic segmentation and deeper slab segmentation, or vice versa. The important implication is that the segmentation of slab geometry at intermediate depth may affect the mechanical coupling at shallower depth.

Acknowledgements

We thank J. Given for helping us use GDSN records at a very early stage of this study, I. Nakanishi for the program to calculate source-process time, and S. Stein for helping collect the seismograms of the 1966 event. B. Isacks sent us a copy of Malthelot's Ph.D. Thesis. D. Wiens led our attention to the effects of water reverberation, and M. Riedesel read an early version of the manuscript. D. Lyle patiently typed this manuscript. This research was supported by NSF grants EAR-8518649 and EAR-8410352 (FT) at the University of Texas and EAR-870835 (LJR) at the University of Michigan. Contribution no. 801 of the Institute for Geophysics at the University of Texas at Austin.

Appendix

We briefly describe the two inversion methods (Ruff and Kanamori, 1983; Kikuchi and Fukao, 1985) discussed in the text. The teleseismic P-wave seismogram for a shallow double-couple point source is given by

$$w(t) = \frac{R}{4\pi\bar{\rho}\alpha^3}\left(\frac{1}{r_0}\right)\left[s(t) + R_{pP}s(t-\Delta t_{pP}) + \frac{\eta_\alpha}{\eta_\beta}R_{sP}s(t-\Delta t_{sP})\right] * Q(t) * I(t) \quad \text{(A1)}$$

where time is measured from the initial arrival of the P-wave ($1/r_0$) denotes the geometrical spreading factor and R is a receiver function either for a vertical component or a horizontal one (see the explanations of the parameters in Langston and Helmberger (1975) and Kanamori and Stewart (1976)). Let $m(t)$ be the source-time function. Then, eqn. (A1) can be shortened to

$$w(t) = g(t;\Delta,\phi,h) * m(t) \quad \text{(A2)}$$

Here $m(t) = M(t)$, the source-time function, and $g(t;\ \Delta,\ \phi,\ h)$ is referred to as the 'half-space' Green's function for a particular mechanism (Ruff and Kanamori, 1983). For a large event, the point source approximation is no longer valid and we need to integrate the contributions from point sources distributed over the fault plane:

$$w(t) = \iint_A g(t;\ \Delta,\ \phi,\ h) * \mu\dot{D}(t)\ \mathrm{d}A \quad \text{(A3)}$$

where $\dot{D}(t)$ is a time derivative of the displacement of a point source, $g(t;\ \Delta,\ \phi,\ h)$ will vary over the fault plane, and yields the directivity effect due to the variation in Δ, ϕ and h across the fault plane. Ruff and Kanamori (1983) (also see Ruff, 1983) assumed that the variation in $g(t)$ over the fault surface is small and took an average of $g(t)$ outside the integral

$$w(t,\ \Delta,\ \phi) = \bar{g}(t;\ \Delta,\ \phi,\ h) * \mu\iint_A \dot{D}(t)\ \mathrm{d}A \quad \text{(A4)}$$

We rewrite eqn. (A4), describing the moment rate function as $m(t) = \mu\int\int_A \dot{D}(t)\ \mathrm{d}A$, i.e.,

$$w(t) = \int_0^\infty g(t-t')m(t')\ \mathrm{d}t' \quad \text{(A5)}$$

To obtain a solution for the time history $m(t)$ in eqn. (A5), Ruff and Kanamori (1983) used the inversion procedure of Backus and Gilbert (1970). Here the functions $w(t)$, $g(t)$ and $m(t)$ are discretized, and accordingly the integral is changed into the following summation with an equal sampling interval:

$$w_j = \sum_{j=1}^{i} g_{i-j+1}m_j \quad \text{(A6)}$$

The solution is obtained to construct an inverse to $\mathbf{A} = [A_{ij}]$, where $A_{ij}\ m_j = w_i$ with $i = 1$ to n. In the analysis the directivity effect which appeared in the deconvolved station-time functions is examined to locate distinct events during the source process.

The 2-D inversion algorithm of Kikuchi and Fukao (1985) is basically the same as that developed by Kikuchi and Kanamori (1982), in which a series of point sources are iteratively determined in a least-squares sense. However, the 2-D inversion includes the variation of Green's function $g(t)$ in eqn. (A3) over the fault surface for a fixed mechanism. Before the iteration, we set grid points at 20-km intervals on a rectangular fault surface

which is defined by the strike and dip directions, and generate a synthetic wavelet for a point source at each grid point. After a set of synthetic wavelets are given for all the stations, the point sources are iteratively determined so that the wavelets best fit the residuals of observed records, i.e. a series of point sources $(m_i,\ t_i,\ x_i,\ y_i)$ $(i = 1,2,\ldots,\ n)$ are determined so that the approximation error

$$\Delta = \sum_{j=1}^{M} \int \left[x_j(t) - m_i w_j(t - t_1;\ x_i,\ y_i) \right]^2 \mathrm{d}t \quad (i = 1,2,\ldots,\ n) \tag{A7}$$

is at a minimum, where M is the number of records. Here the time history of an individual source is described with a trapezoidal time function defined by two time constants τ_1 and τ_2 as follows:

$$s(t) = \begin{cases} t/\tau_1\tau_2 & 0 \le t \le \tau_1 \\ 1/\tau_2 & \tau_1 \le t \le \tau_2 \\ (\tau_1 + \tau_2 - t)/\tau_1\tau_2 & \tau_2 \le t \le \tau_1 + \tau_2 \\ 0 & \text{otherwise} \end{cases}$$

References

Backus, G. and Gilbert, F., 1970. Uniqueness in the inversion of inaccurate gross Earth data. Phil. Trans. R. Soc. Ser. A, 266: 123–192.

Beck, S.L. and Ruff, L.J., 1984. The rupture process of the great 1979 Colombia earthquake: evidence for the asperity model. J. Geophys. Res., 89: 9281–9291.

Bullen, K.E., 1953. An Introduction to the Theory of Seismology. Cambridge University Press, Cambridge, 2i6 pp.

Christensen, D.H. and Ruff, L.J., 1985. Analysis of the trade-off between hypocentral depth and source–time function. Bull. Seismol. Soc. Am., 75: 1637–1656.

Furumoto, M., 1979., Initial phase analysis of R waves from great earthquakes. J. Geophys. Res., 84: 6867–6874.

Furumoto, M. and Nakanishi, I., 1983. Source times and scaling relations of large earthquakes. J. Geophys. Res., 88: 2191–2198.

Habermann, R.E., 1984. Spatial seismicity variations and asperities in the New Hebrides seismic zone. J. Geophys. Res., 82: 5891–5903.

Kanamori, H., 1977. Seismic and aseismic slip along subduction zones and their tectonic implications. Deep Sea Trenches and Back-Arc Basins. Maurice Ewing Series 1, Am. Geophys. Union, 163–174.

Kanamori, H. and Anderson, D.L., 1975. Theoretical basis of some empirical relations in seismology, Bull. Seismol. Soc. Am., 65: 1073–1095.

Kanamori, H. and Given, J.W., 1981. Use of long-period surface waves for rapid determination of earthquake source parameters. Phys. Earth Planet. Inter., 27: 8–31.

Kanamori, H. and Stewart, G.S., 1976. Mode of the train release along the Gibbs fracture zone, Mid-Atlantic Ridge. Phys. Earth Planet. Inter., 27: 8–31.

Kawakatsu, H., 1986. Double seismic zones: kinematics. J. Geophys. Res., 91: 4811–4825.

Kikuchi, M. and Fukao, Y., 1985. Iterative deconvolution of complex body waves from great earthquakes—the Tokachi-oki earthquake of 1968. Phys. Earth Planet. Inter., 37: 235–248.

Kikuchi, M. and Kanamori, H., 1982. Inversion of complex body waves. Bull. Seismol. Soc. Am., 72: 491–506.

Langston, C.A. and Helmberger, C.V., 1975. A procedure for modeling shallow dislocation sources. Geophys. J.R. Astron. Soc., 42: 117–130.

Malthelot, J.-M., 1983. Patterns of seismicity in the Vanuatu (New Hebrides) arc: regional variation and systematic evolution. Ph.D. Thesis, Cornell University.

McCann, W.R., Nishenko, S.P., Sykes, L.R. and Krause, J., 1979. Seismic gaps and plate tectonics: seismic potential for major boundaries. Pure Appl. Geophys., 117: 1082–1147.

Minster, J.B. and Jordan, T., 1980. Present-day Plate Motions: A Summary. Source Mechanism and Earthquake Prediction. Editions du Centre National de la Recherche Scientifique, pp. 109–124.

Peterson, E.T. and Seno, T., 1984. Factors affecting seismic moment release rates in subduction zones. J. Geophys. Res., 89: 10233–10248.

Ruff, L., 1983. Fault asperities inferred from seismic body waves. Earthquakes: Observation, Theory and Interpretation, Proc. Int. School of Physics Enrico Fermi, course LXXXV, pp. 251–276.

Ruff, L. and Kanamori, H., 1983. The rupture process and asperity distribution of three great earthquakes from long-period diffracted P-waves, Phys. Earth Planet. Inter., 31: 202–230.

Schwartz, S. and Ruff, L., 1985. The 1968 Tokachi-Oki and the 1969 Kurile Islands earthquakes: variability in the rupture process, J. Geophys. Res., 90: 8613–8626.

Sykes, L.R. and Quittmeyer, R.C., 1981. Repeat times of great earthquakes along simple plate boundaries, Earthquake Prediction, Maurice Ewing Series 4, Am. Geophys. Union, 217–247.

Tajima, F. and Célérier, B., 1989. Possible focal mechanism change during reactivation of a previously ruptured subduction zone and stress tensor implications. Geophys. J. Int., 98: 301–316.

Tajima, F. and Kanamori, H., 1985. Global survey of aftershock area expansion patterns, Phys. Earth Planet. Inter., 40: 77–134.

Wiens, D.A., 1989. Bathymetric effects on body waveforms from shallow subduction zone earthquakes and application to seismic processes in the Kurile trench. J. Geophys. Res., 94: 2955–2972.

Wyss, M., Habermann, R.E. and Heiniger, C.H., 1983. Seismic quiescence, stress drops, and asperities in the New Hebrides Arc. Bull. Seismol. Soc. Am., 73: 219–236.